IOP Publishing Measurement Science and Technology
Meas. Sci. Technol. **31** (2020) 045017 (17pp) https://doi.org/10.1088/1361-6501/ab5e43

Sparsity enhancement post-nonlinear blind deconvolution method and its application to aluminum honeycomb panel cabin structure

Teng Gong, Zhousuo Zhang[1], Xin Luo, Yanfei Guo and Jianbin Cao

State Key Laboratory for Manufacturing Systems Engineering, Xi'an Jiaotong University, Xi'an 710049, People's Republic of China

E-mail: zzs@xjtu.edu.cn

Received 3 September 2019, revised 8 November 2019
Accepted for publication 3 December 2019
Published 17 January 2020

Abstract

In this paper, we propose a method for post-nonlinear blind source separation. The method divides the separation process of post-nonlinear mixed signals into two independent stages: the nonlinear compensation stage and the linear blind source separation stage. The nonlinear compensation stage is achieved by taking sparsity enhancement as the optimization objective. The $L1$-norm is taken as the objective function and is combined with the fast iteration based on the gradient descent method to realize the fast nonlinear compensation of the mixed signals. In the stage of linear blind source separation, the blind deconvolution algorithm with reference signals is used to process the compensated signals to realize the separation of the source signals. The separation performance of the method is verified by simulation, and the superiority of the method is tested by comparison. The proposed method is also investigated by the excitation experiment of the aluminum honeycomb panel cabin structure, which simulates the satellite structure.

Keywords: post-nonlinear blind source separation, sparsity enhancement, fast nonlinear compensation, blind deconvolution, aluminum honeycomb panel cabin structure

(Some figures may appear in colour only in the online journal)

1. Introduction

Obtaining the pure vibration source signals of the mechanical system is of great significance for the identification of the vibration source state and the formulation of vibration suppression measures. However, it is difficult to directly measure the source signals because each part of the mechanical system will interfere with each other, which makes the signals measured by the sensors the superposition of multiple vibration sources. In order to acquire source information from mixed signals and improve the accuracy of the identification, many signal processing methods have been applied, such as wavelet transform [1], empirical mode decomposition [2], and variational mode decomposition [3, 4]. However, these methods may fail when different sources contain similar or cross-frequencies. Blind source separation (BSS) provides a new way of source recovery, which can extract the source signals from the mixed observation signals without or merely with a small amount of prior knowledge. It has been widely used in vibration source identification and mechanical system analysis. Bouguerriou *et al* studied the application of the BSS method based on second-order statistics in bearing fault diagnosis, and effectively identified bearing defect features [5]. Zhang *et al* proposed the simplified independent component analysis algorithm with reference, and applied it to the source contribution quantitative calculation of mechanical systems [6]. These methods are all for the linear system. However, more and more studies focus on nonlinear models, among which the post-nonlinear (PNL) model has received considerable attention.

In the PNL model, the mixing process comprises an initial linear mixing stage followed by a set of component-wise

[1] Author to whom any correspondence should be addressed.

nonlinear functions [7]. Jutten *et al* proposed the PNL mixed model and proved that the solution of post-nonlinear BSS (PNLBSS) is unique without considering the indeterminacies of scaling and permutation [8]. In the past few decades, PNLBSS has been applied in mechanical systems [9], intelligent sensor array design [10], biomedical signal processing [11] and image processing [12]. The above methods jointly optimize the nonlinear compensation parameters and unmixing parameters under the guidance of the objective function, which can be called joint approaches, and are all for the instantaneous mixing model. However, for complex mechanical systems, the mixing process of the vibration signals is more in line with the convolution mixing model, while the joint approaches cannot be directly applied to the convolution mixing model. Alternatively, in the two-stage approach, an initial stage aims at estimating the nonlinear functions or their inverses. Once these functions are estimated, the second stage simply becomes a linear blind deconvolution (LBD) problem, in which many well-established algorithms can be directly used, resulting in strong applicability. Therefore, the research in this paper is based on the two-stage approach.

The nonlinear compensation stage is at the very core of PNLBSS. In practical applications, there are many cases in which the observed signal is derived from the signal of interest by nonlinear distortion, such as satellite communications [13] and chemical sensors [14]. Usually, the compensation of these nonlinear distortions is carried out by considering a supervised framework [15]. However, this paper focuses on blind signal processing, in which one only has access to the observed signals and a small amount of prior information. Therefore, blind nonlinear compensation must be considered. Zhang *et al* chose the mutual information as the measurement to develop a nonlinear compensation learning algorithm based on the assumption that the distribution of the linear mixture of independent sources is Gaussian [16]. However, the Gaussianization-based methods provide better results as the number of sources increases, while this is not satisfactory for a small number of sources. Dogancay *et al* take minimizing the out-of-band energy at its output as the objective function based on the assumption that nonlinear distortion of band-limited signals results in spectral spreading [17]. But this method has the drawback that the precise bandwidth of the original signal is not always known. Duarte *et al* extend the above method and carry on the nonlinear compensation using $L0$-norm as the objective function based on the assumption that the desired signal admits a sparse representation in a transformed domain and that a nonlinear distortion tends to generate signals that are less sparse than the desired one [18]. Since $L0$-norm is a discontinuous function, smoothed $L0$-norm is proposed as a sparsity measure to overcome this problem [19]. However, other free parameters will be introduced, and there is still the problem that $L0$-norm is sensitive to noise. $L1$-norm is often used to measure signal sparsity because of its simple solution and high robustness to noise [20]. Therefore, this paper takes $L1$-norm as the objective function to enhance the sparsity of the compensated signal, realizing the nonlinear compensation.

The signals after nonlinear compensation are approximate linear mixed signals. In practical applications, especially for complex mechanical systems, observed mixed signals are often the convolutional mixing of source signals. In order to extract the source signals, the blind deconvolution algorithm is needed. After years of development, many mature and effective algorithms have been proposed. Thomas *et al* transformed the convolution mixing process into a time-delay form and proposed the fast multi-channel blind deconvolution algorithm based on FastICA [21]. Belaid and Hattay *et al* proposed an improved blind deconvolution algorithm based on multi-scale decomposition and wavelet transform [22]. In recent years, blind deconvolution with reference (BDR) has received extensive attention because of the improvement of the accuracy of separation by exploiting the prior information. By constructing the contrast function with reference based on the fourth-order cumulant and introducing the optimal step-based optimization algorithm for the maximization of the contrast function, Castella and Moreau proposed a multiple-input single-output (MISO) deconvolution algorithm for single-source signal extraction [23]. In the linear blind deconvolution stage, we combine the MISO deconvolution algorithm with the so-called deflation procedure [24] to extract the source signals iteratively one by one.

In this paper, we propose a novel method of PNL blind deconvolution, which is named the sparsity enhancement post-nonlinear blind deconvolution (SEPNBD). Based on the two-stage framework, the post-nonlinear blind deconvolution is divided into two independent stages: the nonlinear compensation and the linear blind deconvolution. In the nonlinear compensation stage, in view of the fact that the signal in mechanical engineering is usually sparse in the frequency domain and the nonlinear distortion will weaken the sparsity, the sparsity enhancement objective function based on $L1$-norm is constructed and the iterative algorithm is derived. In the linear blind deconvolution stage, the multi-channel blind deconvolution algorithm with reference is used to extract the source signals from the compensated signals. The effectiveness and superiority of the method are verified by simulation analysis. Referring to the actual satellite cabin structure, the satellite scaled model is built with the aluminum honeycomb sandwich panel commonly used in the real satellite. On this basis, an experimental system is established to verify the effectiveness of applying the method for identifying satellite micro-vibration sources.

The remainder of the paper is organized as follows: section 2 presents the theory of the proposed method; in section 3, the performances of the proposed method are illustrated through simulations analysis, and then its effectiveness is further verified by experimental studies in section 4. Conclusions are drawn in section 5.

2. Implementation of sparsity enhancement post-nonlinear blind deconvolution

2.1. Nonlinear blind deconvolution model

For the post-nonlinear instantaneous mixing model, the mixed signals can be expressed as follows:

$$x_j(t) = f_j\left(\sum_{i=1}^{n} a_{ij}s_i(t)\right) \quad i = 1,\cdots,n \quad j = 1,\cdots,m \tag{1}$$

where $x_j(t)$ denotes the mixed observation signal measured by the jth sensor; f_j denotes jth nonlinear distortion function; a_{ij} denotes the linear mixing coefficient from the ith source to the jth observation; $s_i(t)$ denotes the ith source signal; m is the number of mixed observation signals; n is the number of source signals.

This paper focuses on the blind source separation of post-nonlinear convolution mixed signals. The mixed signals can be expressed as follows:

$$x_j(t) = f_j\left(\sum_{i=1}^{n}\sum_{l=0}^{L-1} h_{ij}(l)\, s_i(t-l)\right) \tag{2}$$

where $h_{ij}(l)$ denotes the linear mixing filter coefficient from the ith source to the jth observation; L is the linear mixing filter length.

It can be expressed in matrix form:

$$\boldsymbol{x} = \boldsymbol{F}(\boldsymbol{H} * \boldsymbol{s}) \tag{3}$$

where $\boldsymbol{x} = (x_1, x_2, \cdots, x_m)^T$ denotes the m-dimensional mixed signals measured by sensors;$\boldsymbol{s} = (s_1, s_2, \cdots, s_n)^T$ denotes the n-dimensional source signals; $\boldsymbol{F}$ denotes the m-dimensional nonlinear distortion functions; $\boldsymbol{H}$ denotes the linear mixing filter matrix; $*$ is the symbol of convolution operation.

The purpose of the post-nonlinear blind deconvolution is to obtain the set of nonlinear compensation functions $\boldsymbol{G} = [g_1(\cdot), g_2(\cdot), \cdots, g_m(\cdot)]^T$ and the separation filter matrix $\boldsymbol{W}$, so as to obtain the estimated source signals:

$$\boldsymbol{y} = (y_1, y_2, \cdots, y_n)^T = \boldsymbol{W} * \boldsymbol{G}(x) \tag{4}$$

where $\boldsymbol{y}$ denotes the optimal estimation of source signals.

The separation signal and the source signal can be expressed as

$$y_i(t) = \lambda_i s_j(t - d_i) \tag{5}$$

where λ_i and d_i represent the scaling indeterminacy and the time delay indeterminacy respectively; subscales of y_i and s_j are not necessarily equal to each other, which represents the permutation indeterminacy.

In this paper, the two-stage framework for PNL blind deconvolution is presented, in which nonlinear compensation and linear blind deconvolution are two independent stages.

In the nonlinear compensation stage, the nonlinear compensation functions $\boldsymbol{G}$ are obtained to transform nonlinear mixed signals $\boldsymbol{x}$ into approximate linear mixed signals $\boldsymbol{z} = \mathbf{G}(\mathbf{x})$. Nonlinear compensation includes four issues: the parametrization of the nonlinear compensation function $g_j(\cdot)$, objective function, the selection of transform domain and the optimization algorithm. In the linear blind deconvolution stage, the well-established linear blind deconvolution algorithm can be used to extract the source signals $\boldsymbol{y} = \boldsymbol{W} * \boldsymbol{z}$ from the compensated approximate linear mixed signals $\boldsymbol{z}$. The linear blind deconvolution will be introduced in two parts: the extraction method of the single source signal and all source signals extraction combined with deflation procedure.

2.2. Objective function of nonlinear compensation

The core of nonlinear compensation lies in the objective function. Since the nonlinear distortion usually results in many derivative frequencies, the objective of the proposed method is to minimize or eliminate the derivative frequency components. Based on the assumption that the signals of the mechanical system admit sparse representation in the frequency domain, it is obvious that the more derivative frequency components, the less sparse the signals will be in the frequency domain. That is to say, the reduction of the derivative frequency components is equivalent to the enhancement of sparsity. The proposed method takes the $L1$-norm based objective function to enhance the sparsity of compensated signal $\boldsymbol{z}$, realizing the nonlinear compensation.

The nonlinear compensation operation $z_j = g_j(x_j)$ of each mixed signal x_j is carried out independently. For the simplicity of expression, x, z, $g(\cdot)$ is used to represent each source signal x_j, each compensated signal z_j and each compensation function $g_j(\cdot)$ respectively.

The $L1$-norm of the signal z in its sparse domain is measured by

$$\begin{gathered} \|Z\|_1 = \sum_{j=1}^{N} |Z(j)| \\ s.t. zz^T = 1 \end{gathered} \tag{6}$$

where $Z(j)$ is the coefficient of the signal z in its sparse domain; $\|\cdot\|_1$ denotes the $L1$-norm; N is the sampling number. The energy of z needs to be constrained by normalization of $zz^T = 1$.

The mechanical signals are usually sparse in the frequency domain, so the frequency-related domain is selected as the transform domain. Discrete cosine transform (DCT) and discrete Fourier transform (DFT) are two common frequency-related transforms, both of which can be implemented in matrix form as follows:

$$Z = z\Phi \tag{7}$$

where Φ is the matrix associated with a given linear transform.

DCT is a real transform, which may simplify further optimization, while the coefficients of the DFT are complex. Therefore, the DCT domain is always selected, as in [17]. But, the dimension of the matrix Φ is usually very high and the calculation of equation (7) is time-consuming. In this paper, the DFT domain is chosen as the transform domain. By introducing fast Fourier transform (FFT) into the calculation of the algorithm, the running time will be significantly shortened. Moreover, transforming signals into the frequency domain by DFT is more intuitive in a meaningful aspect than DCT.

For the discrete signal, the DFT can be described as

$$Z(k) = \sum_{n=0}^{N-1} z(n) e^{-\mathrm{i}\frac{2\pi}{N}nk}, k = 0, 1, ...N-1 \tag{8}$$

where i denotes the imaginary unit. By setting $\omega = e^{-\mathrm{i}\frac{2\pi}{N}}$, equation (7) can be transformed into the following matrix form:

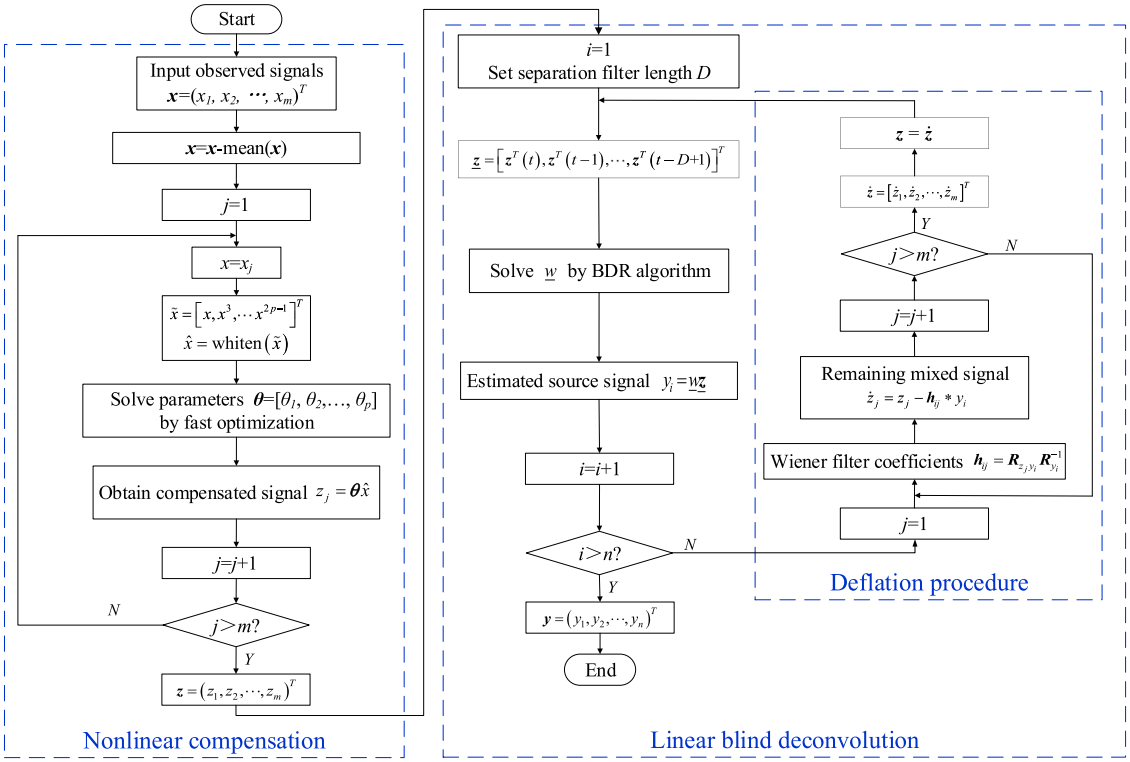

Figure 1. Flowchart of the SEPNBD method.

$$Z = zF^T \tag{9}$$

where

$$Z = [Z(0), Z(1), \cdots, Z(N-1)] \tag{10}$$

$$z = [z(0), z(1), \cdots, z(N-1)] \tag{11}$$

$$F = \begin{bmatrix} \omega^0 & \omega^0 & \cdots & \omega^0 \\ \omega^0 & \omega^1 & \cdots & \omega^{(N-1)} \\ \vdots & \vdots & \ddots & \vdots \\ \omega^0 & \omega^{(N-1)} & \cdots & \omega^{(N-1)(N-1)} \end{bmatrix}. \tag{12}$$

Let $R = \mathrm{Re}(F^T)$ and $I = \mathrm{Im}(F^T)$, then

$$F^T = R + \mathrm{i} \cdot I. \tag{13}$$

Since Z is a complex sequence, its module needs to be calculated before obtaining its $L1$-norm. The modulus of Z can be calculated by

$$|Z| = |z(R + \mathrm{i} \cdot I)| = \sqrt{(zR)^2 + (zI)^2}. \tag{14}$$

For the fitting of the nonlinear compensation functions $g(\cdot)$, multilayer perceptron (MLP) neural network, spline interpolation and polynomial are commonly used models. However, the MLP neural network has the risk of over-fitting [25], and spline interpolation is inconvenient in parameterization. In this paper, the nonlinear compensation function $g(\cdot)$ is fitted by the odd polynomial, since it can provide a flexible enough approximation of the inverse of the distortion function. Further, it is convenient to express the formula, which will show advantages in the subsequent formula derivation. Then the compensated signals z can be expressed as

$$z = g(x) = \sum_{j=1}^{p} \theta_j x^{2j-1} \tag{15}$$

where $\boldsymbol{\theta} = [\theta_1, \theta_2, \ldots, \theta_p]$ is the polynomial coefficients to be solved; p is the polynomial order.

Equation (15) can be expressed in matrix form:

$$z = \boldsymbol{\theta}\tilde{x} \tag{16}$$

where

$$\tilde{x} = \left[x, x^3, \cdots x^{2p-1}\right]^T. \tag{17}$$

Substituting equation (16) into (14) obtains

$$|Z| = |z(R + \mathrm{i} \cdot I)| = \sqrt{(\boldsymbol{\theta}\tilde{x}R)^2 + (\boldsymbol{\theta}\tilde{x}I)^2}. \tag{18}$$

Let us now turn our attention to the constrained condition $zz^T = 1$. It is easy to get

$$\boldsymbol{\theta}\tilde{x}\tilde{x}^T\boldsymbol{\theta}^T = 1. \tag{19}$$

Whitening operation is carried out by linear transformation $\hat{x} = V\tilde{x}$ to satisfy $\hat{x}\hat{x}^T = I$. One popular method for whitening is to use the eigenvalue decomposition (EVD) of the covariance matrix $E\left\{\tilde{x}\tilde{x}^T\right\} = \boldsymbol{E}\boldsymbol{D}\boldsymbol{E}^T$, where $\boldsymbol{E}$ is the orthogonal matrix of eigenvectors of $E\left\{\tilde{x}\tilde{x}^T\right\}$ and $\boldsymbol{D} = \mathrm{diag}(d_1, \ldots, d_n)$ is the diagonal matrix of its eigenvalues [26]. Whitening can be done by

$$\hat{x} = \boldsymbol{E}\boldsymbol{D}^{-1/2}\boldsymbol{E}^T\tilde{x}. \tag{20}$$

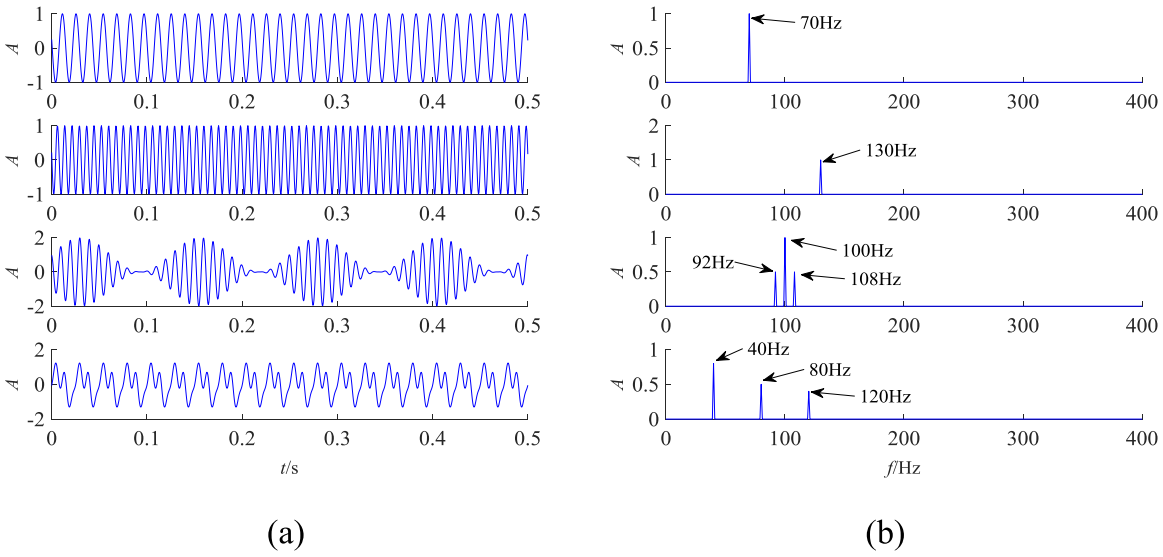

Figure 2. Waveform and spectrums of the source signals $\boldsymbol{s}$. (a) Waveforms, (b) Fourier spectrums.

Then equation (19) can be transformed into $\boldsymbol{\theta}\boldsymbol{\theta}^T = 1$. Therefore, the constrained condition $zz^T = 1$ can be achieved by $\boldsymbol{\theta}\boldsymbol{\theta}^T = 1$ under the condition that $\tilde{x}$ has been whitened to $\hat{x}$.

To sum up, the objective function is set as

$$\min_{\boldsymbol{\theta}} J(\boldsymbol{\theta}) = \sqrt{(\boldsymbol{\theta}\hat{x}R)^2 + (\boldsymbol{\theta}\hat{x}I)^2} \quad \text{s.t.} \quad \boldsymbol{\theta}\boldsymbol{\theta}^T = 1. \tag{21}$$

The objective function is used to adjust the parameters $\boldsymbol{\theta}$ so as to enhance the sparsity of the compensated signal z.

2.3. Fast optimization of nonlinear compensation

By constructing an objective function based on signal sparsity in the frequency domain, the problem of nonlinear compensation is transformed into an optimization problem of objective function minimization. The gradient descent method, as a classical optimization algorithm, is widely used in functional extremum problems. In this paper, the gradient descent method is used to adjust the parameters $\boldsymbol{\theta}$. Because the nondifferentiable of $L1$-norm at 0 point will affect the application of the gradient algorithm, the smoothed $L1$-norm is often used. In this paper, a smoothing parameter δ is introduced into the objective function as follows:

$$J(\boldsymbol{\theta}) = \sqrt{(\boldsymbol{\theta}\hat{x}R)^2 + (\boldsymbol{\theta}\hat{x}I)^2 + \delta}. \tag{22}$$

$\hat{x}R$ and $\hat{x}I$ can be fast calculated by FFT, which avoids a matrix operation with high dimension and improves the efficiency of the algorithm.

The gradient of equation (22) to $\boldsymbol{\theta}$ is

$$\nabla_{\boldsymbol{\theta}} J(\boldsymbol{\theta}) = (\boldsymbol{\theta}\hat{x}R./H_1)(\hat{x}R)^T + (\boldsymbol{\theta}\hat{x}I./H_1)(\hat{x}I)^T \tag{23}$$

where

$$H_1 = \sqrt{(\boldsymbol{\theta}\hat{x}R)^2 + (\boldsymbol{\theta}\hat{x}I)^2 + \delta}. \tag{24}$$

The iteration process is as follows:

$$\boldsymbol{\theta}(k+1) = \boldsymbol{\theta}(k) - \alpha\nabla_{\boldsymbol{\theta}} J(\boldsymbol{\theta}) \tag{25}$$

where $\boldsymbol{\theta}(k)$ denotes the solution of the kth iteration; α is the step size. The normalization process needs to be done after each iteration to ensure the constrained condition $\boldsymbol{\theta}\boldsymbol{\theta}^T = 1$, which can be achieved by

$$\boldsymbol{\theta} = \boldsymbol{\theta}/\|\boldsymbol{\theta}\|_2. \tag{26}$$

Repeat iteration until convergence and the compensated signal can be obtained by

$$z = \boldsymbol{\theta}\hat{x}. \tag{27}$$

The convergence of iteration can be judged by comparing the difference between the value of objective function before iteration and after iteration. If the difference value is less than the given threshold value for convergence, the convergence is achieved.

Therefore, the algorithm steps of nonlinear compensation for one mixed signal are as follows:

(1) Center the original mixed signal x.
(2) Let $\tilde{x} = \left[x, x^3, \cdots x^{2p-1}\right]^T$.
(3) Whiten $\tilde{x}$ to $\hat{x}$.
(4) Calculate $\hat{x}R$ and $\hat{x}I$ by FFT.
(5) Initialize $\boldsymbol{\theta}$ randomly and normalize it by $\boldsymbol{\theta} = \boldsymbol{\theta}/\|\boldsymbol{\theta}\|_2$.
(6) Iterate $\boldsymbol{\theta}$ by equation (25).
(7) Normalize $\boldsymbol{\theta}$ by $\boldsymbol{\theta} = \boldsymbol{\theta}/\|\boldsymbol{\theta}\|_2$.
(8) If $\boldsymbol{\theta}$ has not converged, go back to step (6).
(9) Calculate the compensated signal $z = \boldsymbol{\theta}\hat{x}$.

Through the above process, nonlinear compensation for one mixed signal x_j can be fast realized, obtaining the approximate linear convolution mixed signal z_j. Each mixed signal $x_1, x_2, \cdots, x_m$ is separately operated to get the signals $\boldsymbol{z} = [z_1, z_2, \cdots, z_m]^T$, and then the linear blind deconvolution algorithm can be used to extract the source signals from the signals $\boldsymbol{z}$.

2.4. Single-source signal extraction of LBD

Compensated signals $\boldsymbol{z}$ can be considered as linear convolutive mixtures of source signals $\boldsymbol{s}$, so it can be processed by

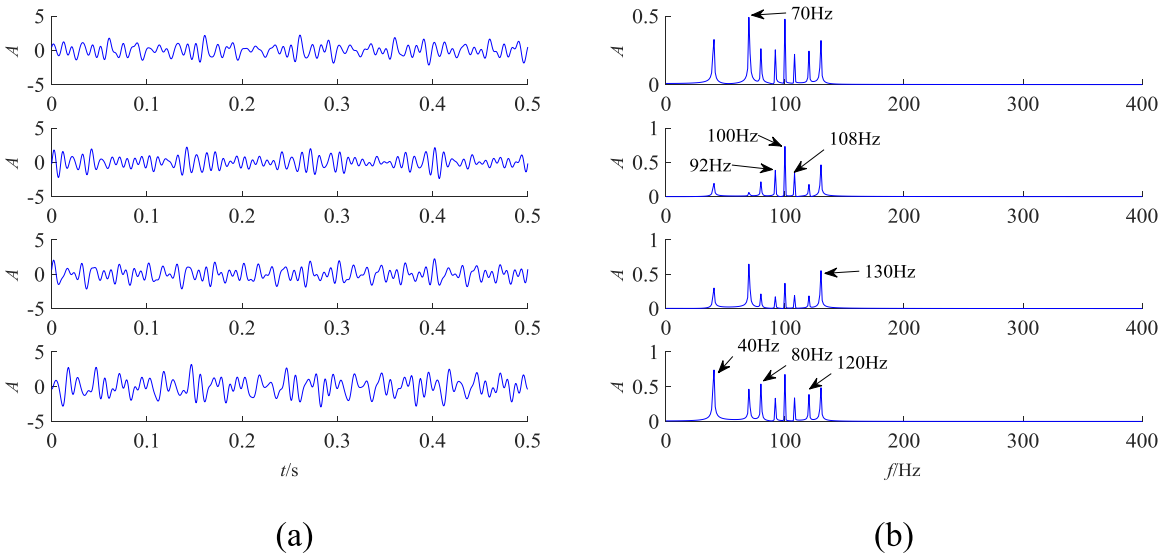

Figure 3. Waveform and spectrums of the signals $\boldsymbol{u}$. (a) Waveforms, (b) Fourier spectrums.

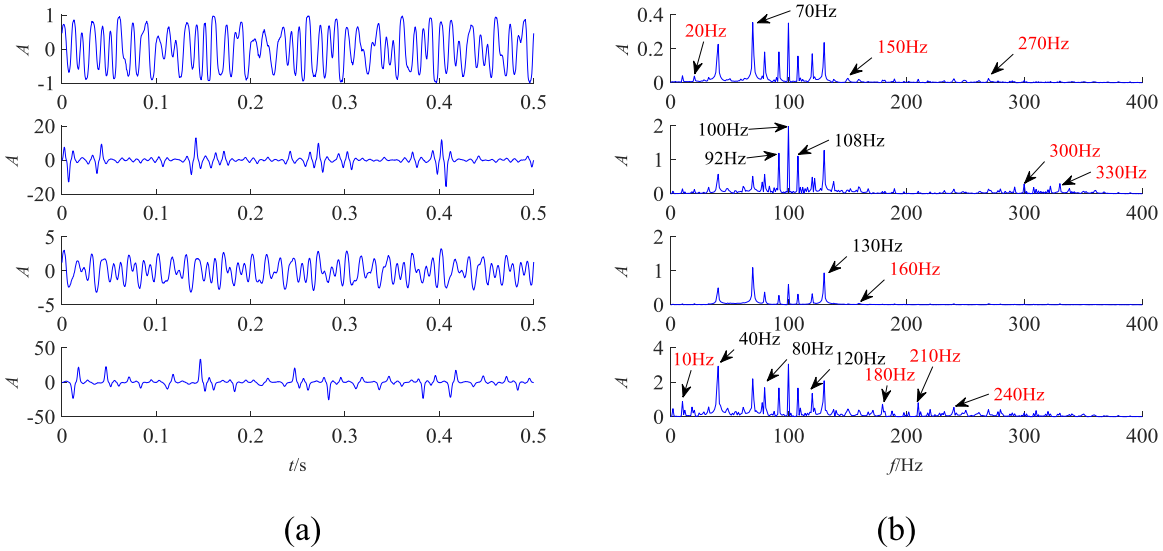

Figure 4. Waveform and spectrums of the mixed signals $\boldsymbol{x}$. (a) Waveforms, (b) Fourier spectrums.

a well-established linear blind deconvolution algorithm. The blind deconvolution algorithm with reference (BDR) [23] is selected in this paper.

The realization process of linear blind deconvolution is

$$y_i(t) = \sum_{j=1}^{m} \sum_{d=0}^{D-1} w_{ij}(d)\, z_j(t-d) \tag{28}$$

where w_{ij} denotes the separation filter; D is the separation filter length.

It can also be written in the form of matrix:

$$\boldsymbol{y} = \boldsymbol{W} * \boldsymbol{z}. \tag{29}$$

The deconvolution model can be transformed into the ICA model:

$$\boldsymbol{y} = \underline{\boldsymbol{W}}\, \underline{\boldsymbol{z}} \tag{30}$$

where

$$\underline{\boldsymbol{W}} = (\boldsymbol{w}(0), \boldsymbol{w}(1), \cdots, \boldsymbol{w}(D-1)) \tag{31}$$

$$\underline{\boldsymbol{z}}(t) = \left(\boldsymbol{z}(t)^T, \boldsymbol{z}(t-1)^T, \cdots, \boldsymbol{z}(t-D+1)^T\right)^T. \tag{32}$$

Linear blind deconvolution can be achieved by a method similar to instantaneous blind source separation.

Taking normalized kurtosis maximization and the optimal step gradient algorithm as the contrast function and optimization algorithm respectively, the single-source signal can be extracted by

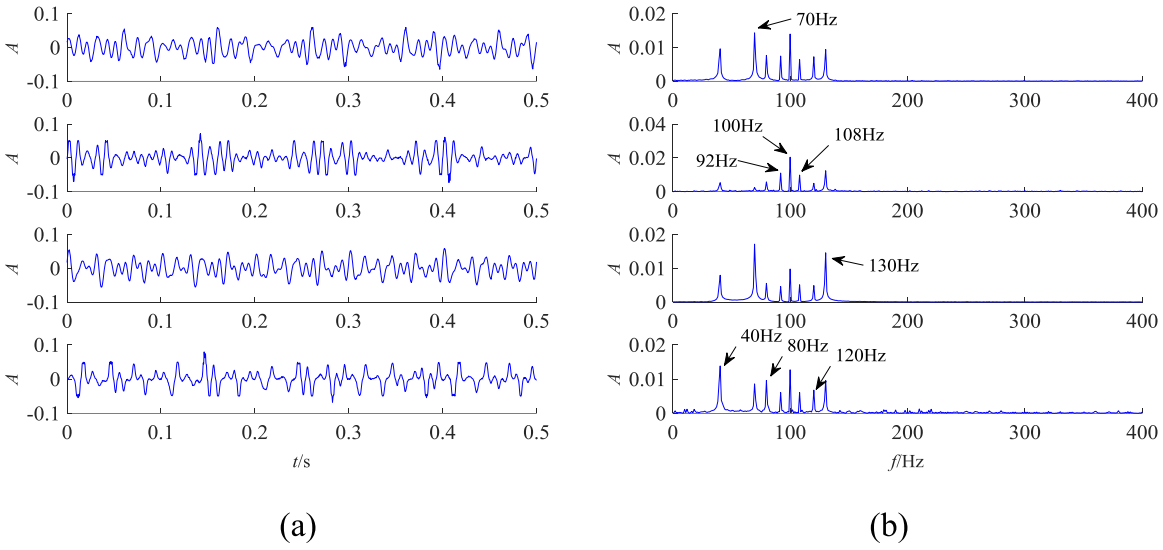

Figure 5. Waveform and spectrums of the compensated signals z. (a) Waveforms, (b) Fourier spectrums.

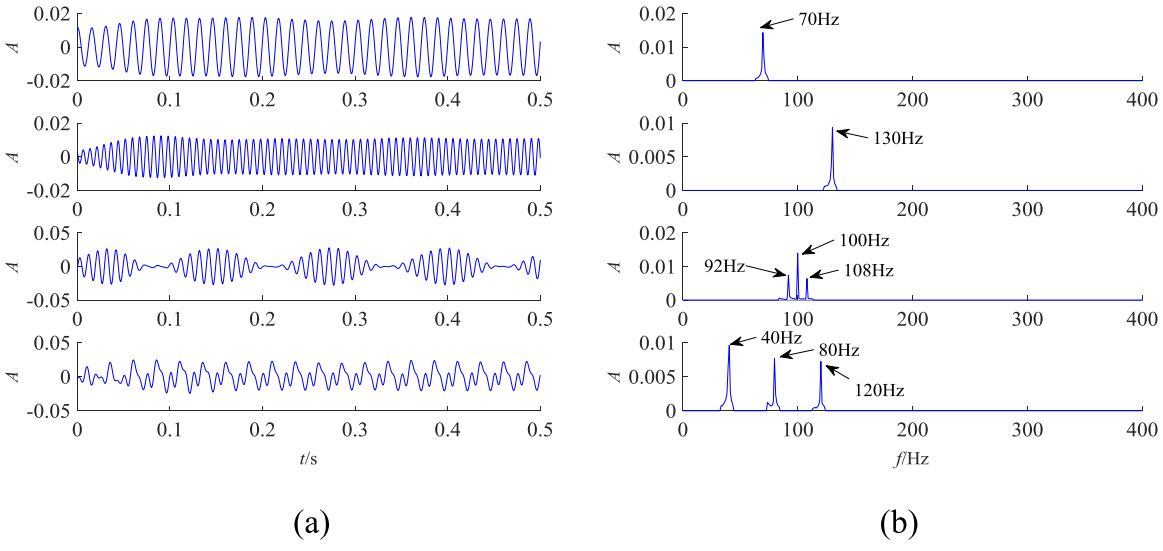

Figure 6. Waveform and spectrums of the reference signals. (a) Waveforms, (b) Fourier spectrums.

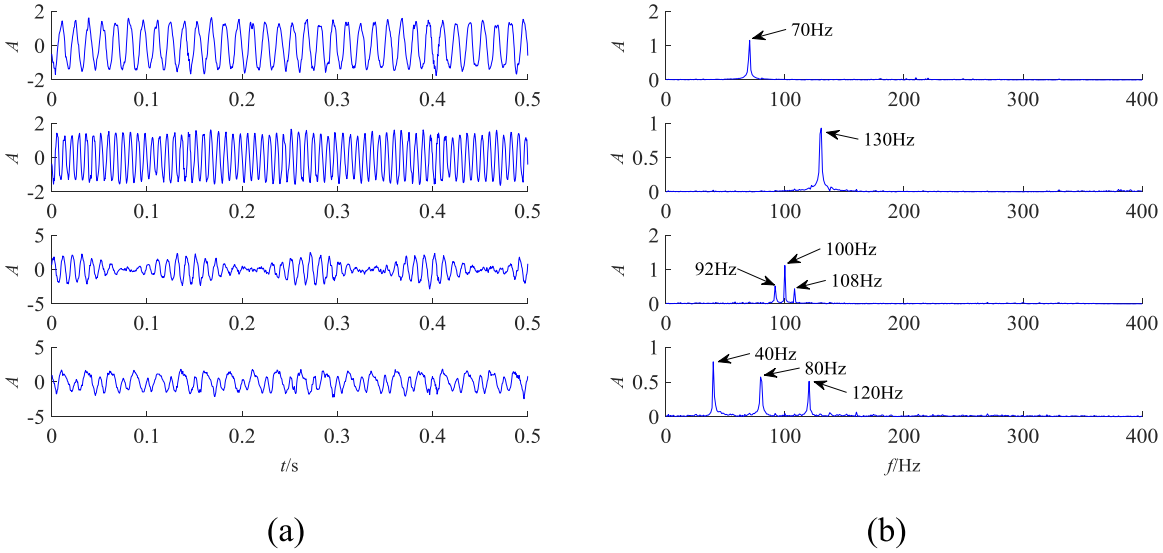

Figure 7. Waveform and spectrums of the separated signals by SEPNBD. (a) Waveforms, (b) Fourier spectrums.

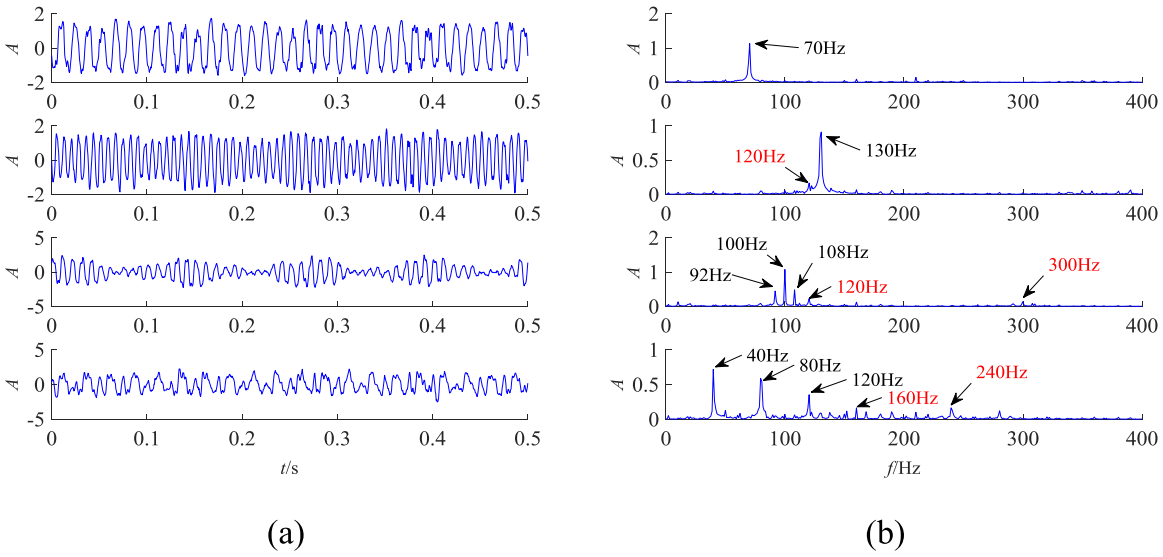

Figure 8. Waveform and spectrums of the separated signals by LBD. (a) Waveforms, (b) Fourier spectrums.

Table 1. Comparison of SCCs of separated signals by different methods.

	SCCs of separated signals				
Methods	$y_1(t)$	$y_2(t)$	$y_3(t)$	$y_4(t)$	Average
Proposed method	0.9928	0.9934	0.9795	0.9655	0.9828
LBD algorithm in [23]	0.9781	0.9816	0.9385	0.8914	0.9474

$$y_i = \underline{w}\underline{z} \tag{33}$$

where $\underline{w}$ is a row of $\underline{\boldsymbol{W}}$.

The normalized kurtosis contrast function is

$$\kappa_r\left(\underline{w}\right) = \left|\frac{C_r\left\{y_i\right\}}{E\left\{\left|y_i\right|^2\right\}E\left\{\left|r_i\right|^2\right\}}\right|^2 \tag{34}$$

where $C_{r_i}\left\{y_i\right\} \triangleq Cum\left\{y_i, y_i^*, r_i, r_i^*\right\}$ denotes the fourth-order cumulant; r_i is the reference signal.

The iterative process is

$$\underline{w}\left(k+1\right) = \underline{w}\left(k\right) + \eta g \tag{35}$$

where $\underline{w}\left(k\right)$ is the kth iteration value of $\underline{w}$; η is the step size; g is the derivative of $\kappa_r\left(\underline{w}\right)$.

The value of step size η can affect the convergence performance of the algorithm. Selecting the optimal step size η_{opt} that can maximize the contrast function in each iteration:

$$\eta_{\text{opt}} = \arg\max_{\eta}\left|\kappa_r\left[\underline{w}\left(k\right) + \eta g\right]\right|. \tag{36}$$

The optimal step size η_{opt} should be such that $\partial\kappa_r\left[\underline{w}\left(k\right) + \eta g\right]/\partial\eta = 0$. It must be calculated in each iteration. Repeat iteration until convergence or the maximum number of iterations is reached. The specific implementation process can be referred to in [23]. Through the above process, we can extract a single separation component y_i, that is, a single-source signal.

2.5. Deflation procedure of LBD

After obtaining one source signal, subtract its contribution from the remaining mixed observed signal. The above process is repeated until all source signals are extracted one by one. This successive extraction method reduces the difficulty of separation and improves the separation accuracy [27].

The subtraction of source signal contribution can be achieved by the Wiener filter. The parameters of the Wiener filter subtracting the ith source signal contribution from the jth remaining mixed signal can be solved by

$$\boldsymbol{h}_{ij} = \arg\min_{h} E\left(\left|z_j - \boldsymbol{h} * y_i\right|^2\right) \tag{37}$$

where $\boldsymbol{h}_{ij} = \left[h_{ij}\left(0\right), h_{ij}\left(1\right), \cdots, h_{ij}\left(N-1\right)\right]$ are the parameters of the Wiener filter; N is the Wiener filter length.

It is deduced from equation (37) that

$$\boldsymbol{h}_{ij} = \boldsymbol{R}_{z_j y_i}\boldsymbol{R}_{y_i}^{-1} \tag{38}$$

where $\boldsymbol{R}_{z_j y_i}$ is a $1 \times N$ vector whose lth element $\boldsymbol{R}_{z_j y_i}\left(l\right) = E\left[z_j\left(t\right) y_i\left(t-l+1\right)\right]$; $\boldsymbol{R}_{y_i}$ is a $N \times N$ matrix in which $\boldsymbol{R}_{y_i}\left(l,m\right) = E\left[y_i\left(t-m\right) y_i\left(t-l\right)\right]$.

Then the remaining mixed observed signal can be expressed as

$$\dot{z}_j = z_j - \boldsymbol{h}_{ij} * y_i. \tag{39}$$

Through the above steps, the signals $\dot{\boldsymbol{z}} = \left[\dot{z}_1, \dot{z}_2, \cdots, \dot{z}_m\right]^T$ can be obtained. Replace the original mixed signal $\boldsymbol{z}$ by the remaining mixed observed signal $\dot{\boldsymbol{z}}$ and then extract the second source signal through the single source extraction method introduced in section 2.4.

Repeat the process until all source signals $\boldsymbol{y} = \left[y_1, y_2, \cdots, y_m\right]^T$ are extracted.

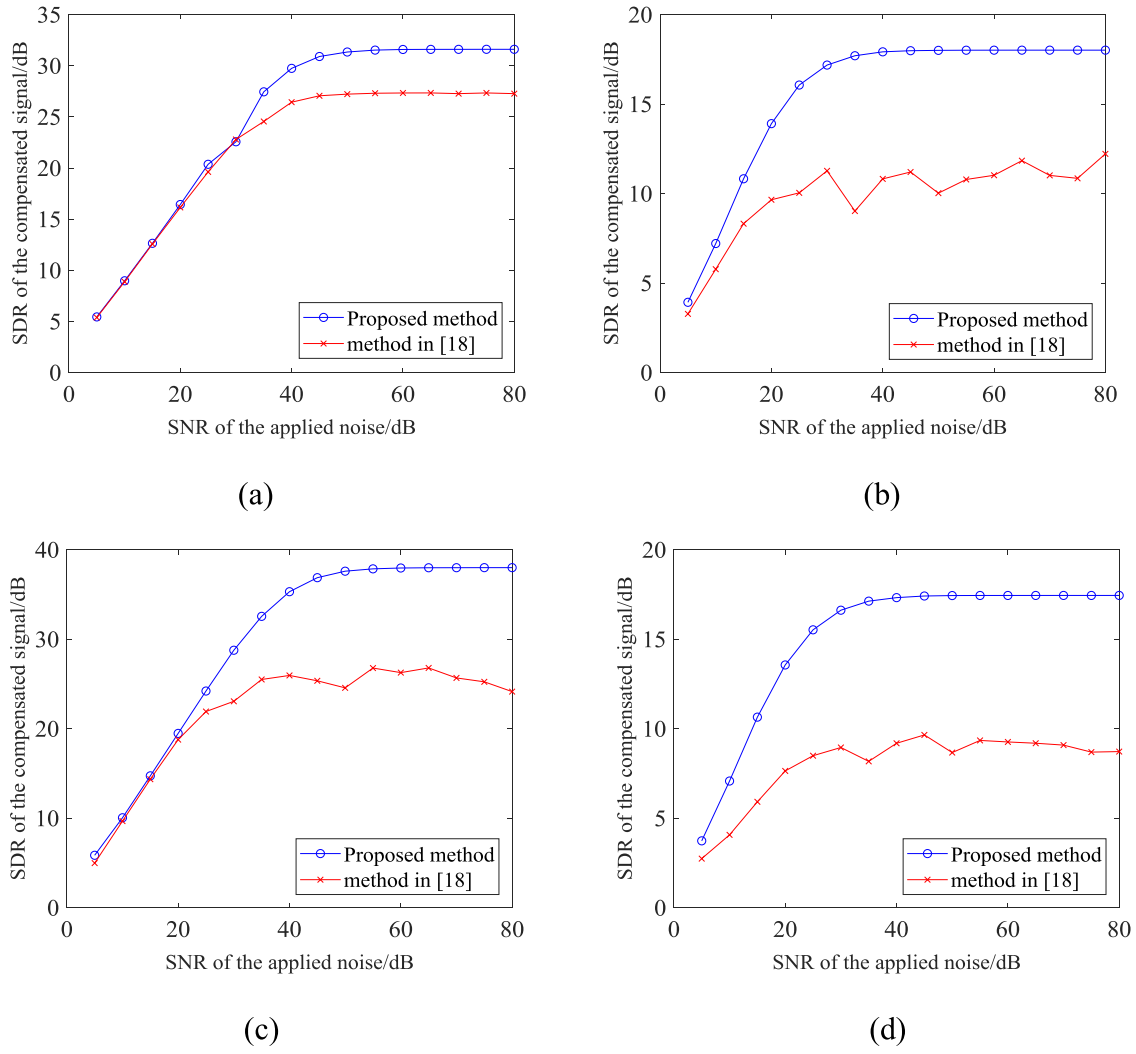

Figure 9. Comparisons of compensation performance. (a) The first nonlinear distortion function $f_1(u)$; (b) the second nonlinear distortion function $f_2(u)$; (c) the third nonlinear distortion function $f_3(u)$; (d) the fourth nonlinear distortion function $f_4(u)$.

2.6. Algorithm flow

To sum up, the nonlinear compensation is realized based on the objective function of sparsity enhancement, and then the compensated signals are processed by the linear blind deconvolution algorithm to extract all source signals, which is called the SEPNBD method. The flowchart of the SEPNBD method is illustrated in figure 1.

3. Simulations analysis

3.1. Effectiveness of the proposed method

In order to validate the effectiveness of the proposed method, evaluate its performance and verify its superiority by comparison, the following simulation is performed.

The following typical signals are selected as simulation signals: $s_1(t)$ is a low frequency sinusoidal wave; $s_2(t)$ is a high frequency sinusoidal wave; $s_3(t)$ is a periodic wave with amplitude modulation; $s_4(t)$ is a multi-component signal. The generating functions of source signals are listed as follows:

$$\mathbf{s}(t) = \begin{bmatrix} s_1(t) \\ s_2(t) \\ s_3(t) \\ s_4(t) \end{bmatrix} = \begin{bmatrix} \sin(2\pi \cdot 70t) \\ \sin(2\pi \cdot 130t) \\ \cos(2\pi \cdot 100t)\,[1 + \sin(2\pi \cdot 8t)] \\ 0.8\sin(2\pi \cdot 40t) + 0.5\sin(2\pi \cdot 80t) + 0.4 \times \sin(2\pi \cdot 120t) \end{bmatrix}. \tag{40}$$

The phases of the signals are generated randomly. The sampling frequency is 2048 Hz and the sampling length is 1 s. Figure 2 shows the waveforms and Fourier spectrums of source signals $\boldsymbol{s}$. In order to intuitively show the characteristics of the signals, the waveforms only show the parts of 0–0.5 s, and the spectrums only show the parts of 0–400 Hz.

Hybrid filter $\boldsymbol{H}$ is a random-generated FIR filter with an order of 20. Convolutive mixtures $\boldsymbol{u} = (u_1, u_2, u_3, u_4)^T$ are obtained by $\boldsymbol{u} = \boldsymbol{H} * \mathbf{s}$ as shown in figure 3.

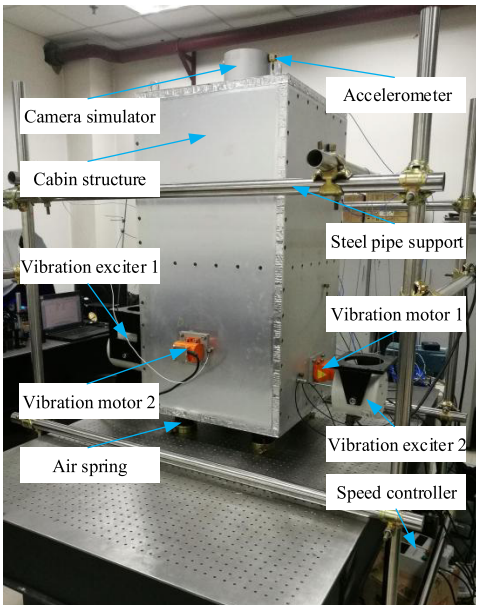

(a)

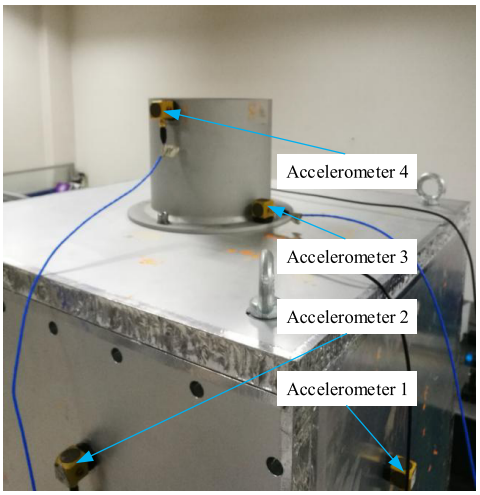

(b)

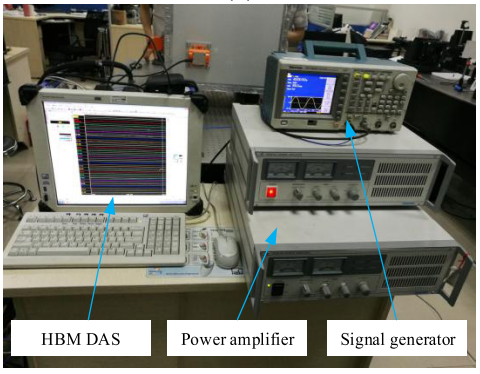

(c)

Figure 10. Photographs of the cabin structure experiment system. (a) Cabin structure; (b) locations of the accelerometers; (c) experimental control system.

In order to verify the applicability of the proposed method to different nonlinear forms, four different nonlinear distortion functions are selected as follows:

$$\boldsymbol{F}(u) = \begin{bmatrix} f_1(u) \\ f_2(u) \\ f_3(u) \\ f_4(u) \end{bmatrix} = \begin{bmatrix} \tanh(u) \\ u + u^3 \\ u + \tanh(u) \\ u^3 + \tanh(u) \end{bmatrix}. \tag{41}$$

The final mixed signals $\boldsymbol{x} = (x_1, x_2, x_3, x_4)^T$ are obtained by applying the nonlinear functions to u_1, u_2, u_3, u_4 in turn and adding 30 dB white noise as shown in Figure 4. As can be seen from figure 4(a), the waveforms have changed significantly. The spectrums in figure 4(b) also show that the nonlinear function can lead to a lot of derivative frequencies, such as 10 Hz, 160 Hz, 240 Hz, 300 Hz.

Firstly, the nonlinear compensation is carried out to the post-nonlinear convolutive mixtures $\boldsymbol{x}$ to get the compensation functions $\boldsymbol{G}$ and compensated signals $\boldsymbol{z}$. Set the odd polynomial order $p = 4$; smoothing parameter $\delta = 10^{-6}$; iterative step size $\alpha = 0.3$; the threshold value for convergence is 10^{-6}. The waveforms and spectrums of the compensated signals $\boldsymbol{z}$ are shown in figure 5. Comparing figure 4 and 5, it is obvious that the derivative frequency components in figure 4 have been mostly eliminated.

Then, the BDR algorithm in [23] is used to process the compensated signals $\boldsymbol{z}$ to extract the source signals. The construction of reference signals is the first step of the BDR algorithm. The reference signals should contain the characteristics of the source signals to be extracted. Harmonic wavelet analysis [28] is used to extract the reference signals from the compensated signals because of its simplicity and high efficiency. As shown in figure 6, the reference signals contain the corresponding source information, which can meet the requirements of the BDR algorithm. The algorithm parameters are set as follows: separation filter length $D = 20$; the maximum number of iterations is 2000; the threshold value for convergence is 10^{-5}. The waveforms and spectrums of the separated signals are shown in figure 7.

Comparing figure 2 and 7, it can be found that the waveforms and spectrums of the separated signals are similar to that of the source signals. The proposed SEPNBD method successfully achieves the separation of vibration source signals from the post-nonlinear convolutive mixtures.

3.2. Performance of the proposed method

The performance of the method is evaluated from three aspects: the performance of nonlinear compensation, the running time of nonlinear compensation, and the separation performance.

The performance of nonlinear compensation is measured by the signal-to-distortion ratio (SDR) in dB, which is defined as

$$\mathrm{SDR} = 10\log\left(\frac{\bar{u}\bar{u}^T}{(\bar{u} - \bar{z})(\bar{u} - \bar{z})^T}\right). \tag{42}$$

$\bar{z} = z/\|z\|_2$ is the normalized z and $\bar{u} = u/\|u\|_2$ is the normalized u. The normalization is necessary because of the scaling indeterminacy in nonlinear compensation. This index measures the similarity between compensation signal z and

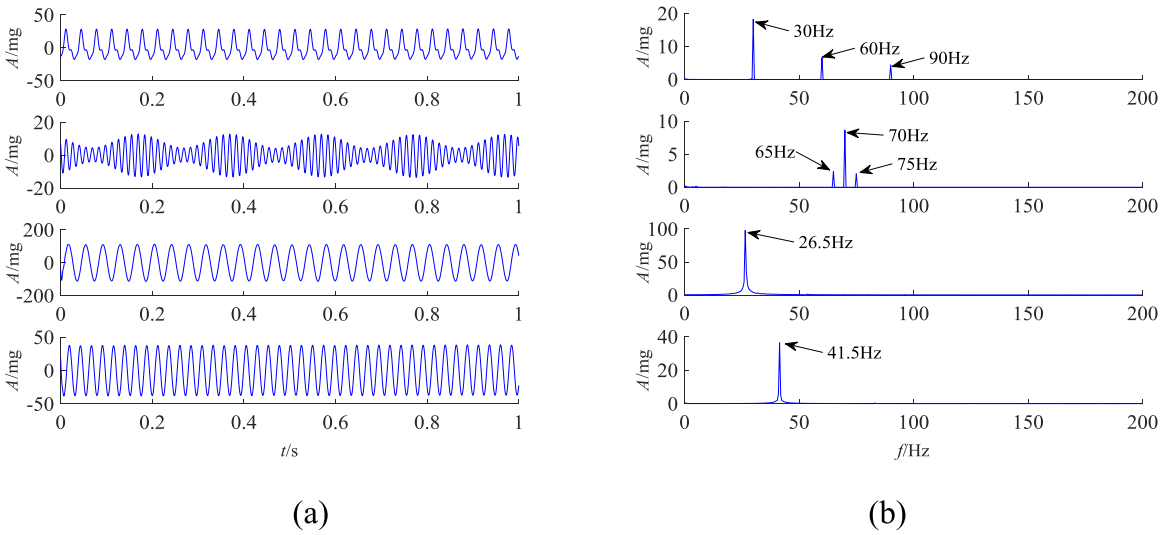

Figure 11. Waveform and spectrums of the source signals $\boldsymbol{s}$. (a) Waveforms, (b) Fourier spectrums.

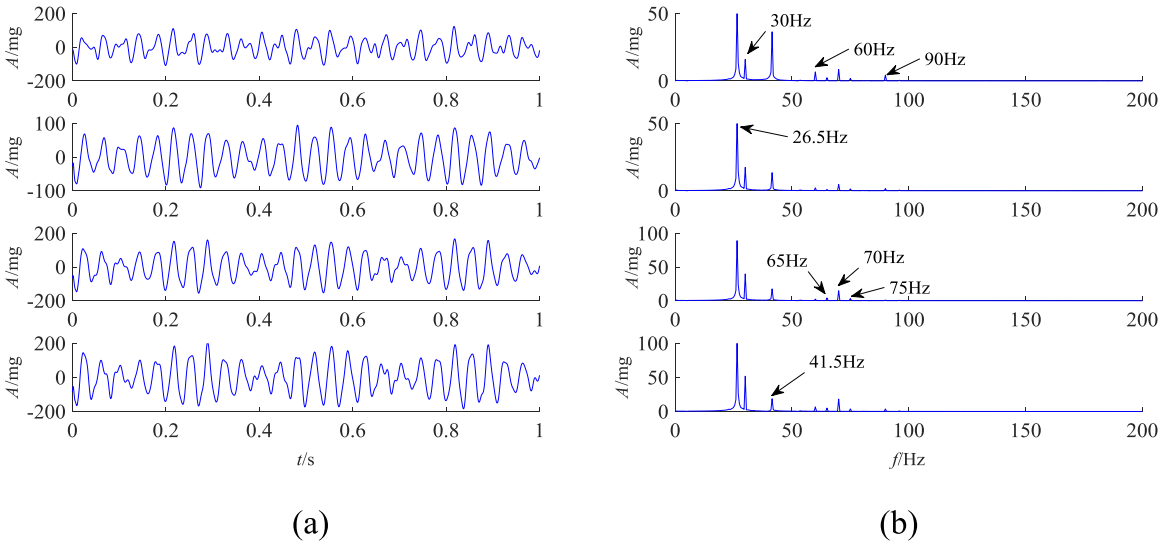

Figure 12. Waveform and spectrums of the mixed signals $\boldsymbol{u}$. (a) Waveforms, (b) Fourier spectrums.

convolutive mixed signal u. The larger the index value, the higher the degree of similarity, indicating a better performance of nonlinear compensation. The SDRs of the four compensated signals are 23.74 dB, 14.49 dB, 28.54 dB and 12.40 dB, respectively.

The running time of the nonlinear compensation process is 0.0279 s, which is the average value of 20 runs. The CPU of the computer is an i3-4150 dual-core processor at 3.50 GHz and the RAM is 8 GB of 1600 MHz DDR3. It is a direct conclusion that the proposed method has the remarkable advantage of high efficiency.

The separation performance is measured by the spectral correlation coefficient (SCC):

$$\mathrm{SCC} = \frac{\sum_{k=1}^{N} |Y(k)|\,|S(k)|}{\sqrt{\sum_{k=1}^{N} |Y(k)|^2 \sum_{k=1}^{N} |S(k)|^2}} \tag{43}$$

where $Y(k)$ and $S(k)$ are the DFT of the signal y and s, respectively; and N is the sampling points.

Table 2. Optimum parameters and resulting RMS errors through various experimental data.

Group number	α	β	RMS errors
1	1.9638	0.9945	0.012
2	1.6623	0.0552	0.041
3	2.1587	1.1517	0.010

This index measures the similarity between the separated signal y and the source signal s. The SCC ranges from 0 to 1. And the closer it is to 1, the better the separation performance is. The SCCs between the separated signals and the corresponding source signals are 0.9928, 0.9934, 0.9795 and 0.9655.

3.3. Superiority of the proposed method

To demonstrate the superiority of the proposed method, it is compared with the LBD algorithm in [23] and the blind compensation method in [18].

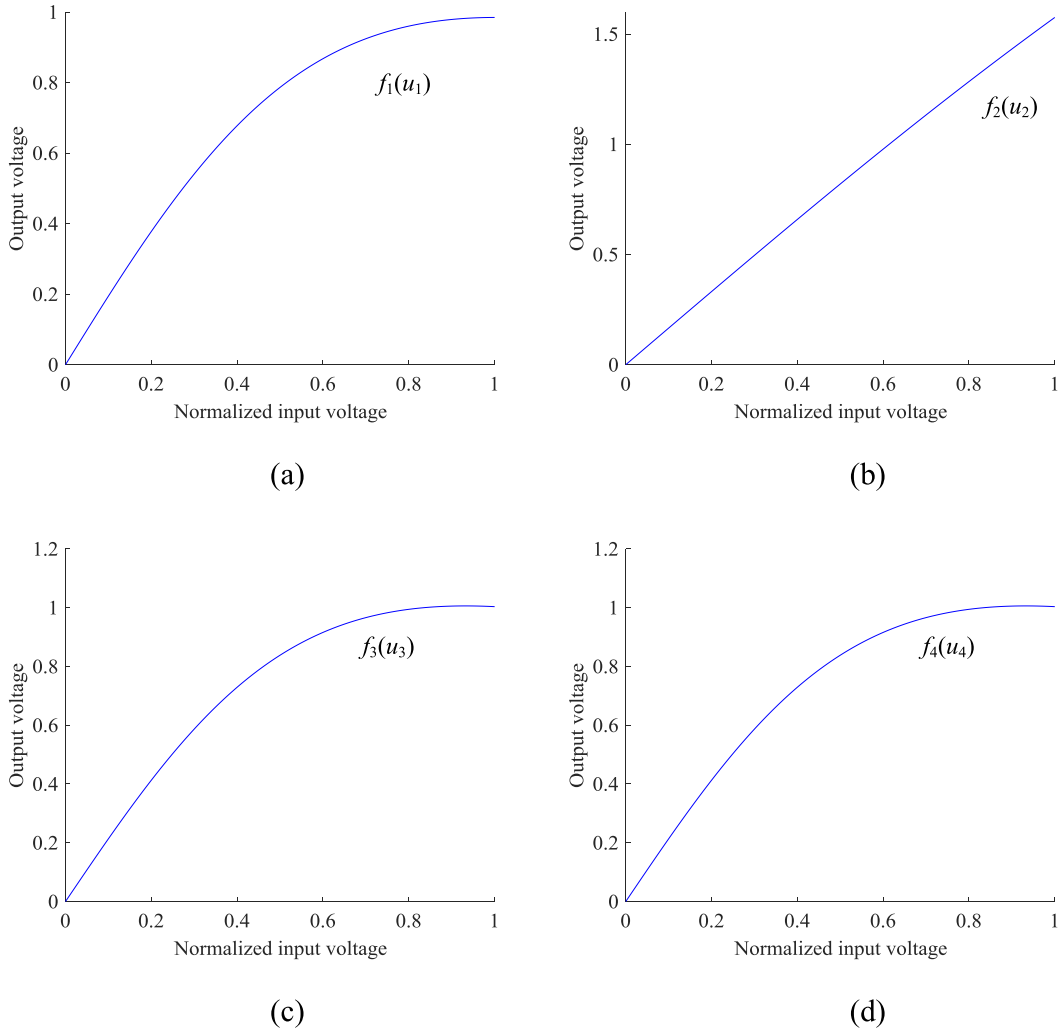

Figure 13. The nonlinear distortion functions. (a) Nonlinear function f_1 for u_1; (b) nonlinear function f_2 for u_2; (c) nonlinear function f_3 for u_3; (d) nonlinear function f_4 for u_4.

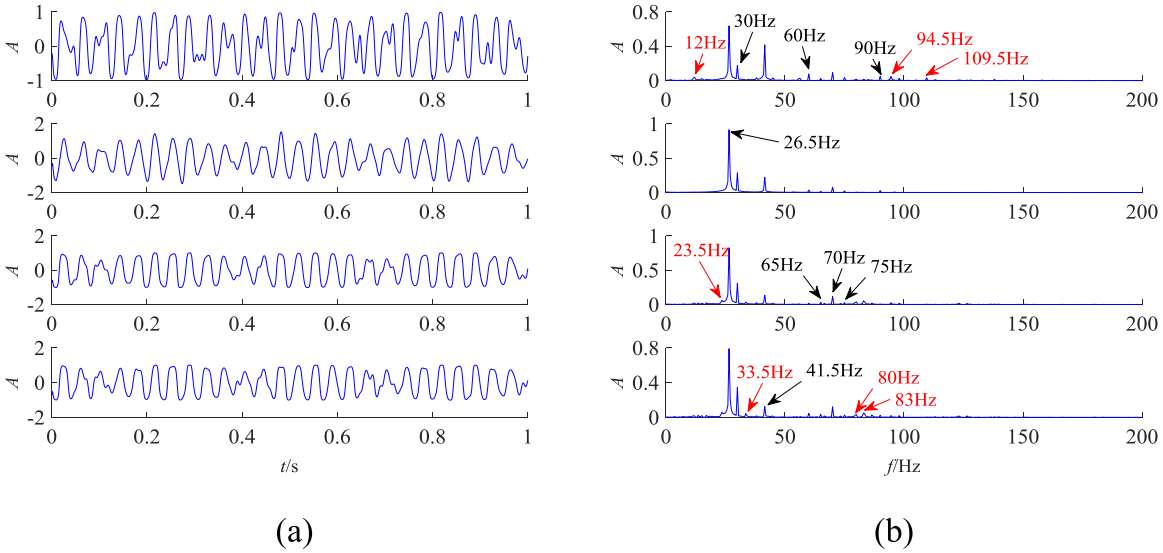

Figure 14. Waveform and spectrums of the post-nonlinear mixed signals. (a) Waveforms, (b) Fourier spectrums.

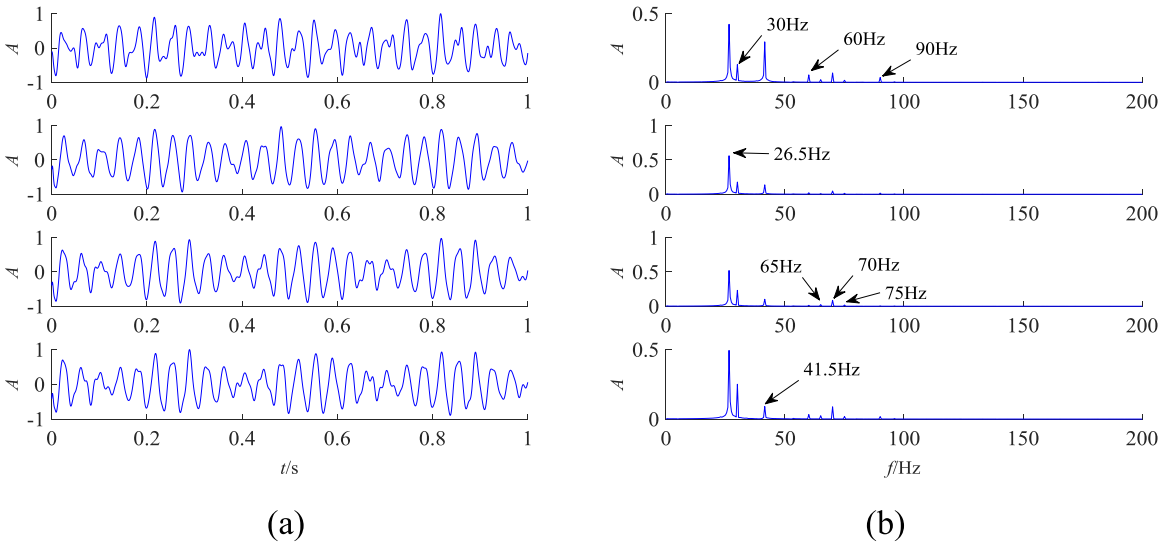

Figure 15. Waveform and spectrums of the compensated signals. (a) Waveforms, (b) Fourier spectrums.

Table 3. Comparison of nonlinear compensation by different methods.

	SDRs of compensated signals (dB)					
Methods	$z_1(t)$	$z_2(t)$	$z_3(t)$	$z_4(t)$	Average	Running time
Proposed method	37.19	31.94	31.28	32.07	33.12	0.1760 s
Method in [18]	33.56	29.92	26.21	26.15	28.96	70.97 s

The LBD algorithm is used to process the post-nonlinear convolutive mixtures $\boldsymbol{x}$ in Figure 4 directly. The algorithm parameters are set as follows: separation filter length $D = 20$; the maximum number of iterations is 2000; the threshold value for convergence is 10^{-5}. The separated signals are obtained as shown in figure 8.

As can be seen in figure 8, there are some cross-frequencies such as 120 Hz and some derivative frequencies such as 160 Hz, 240 Hz, 300 Hz in the Fourier spectrums. Actually, the LBD algorithm in [23] is an effective algorithm for separating linear mixed signals by a separation filter matrix. However, post-nonlinear mixtures are not the linear combination of sources, and thus cannot be well separated merely by a separation filter matrix. Table 1 shows SCCs of separated signals by the proposed method and LBD algorithm. The average SCCs of the proposed method and LBD algorithm are 0.9828 and 0.9474 respectively. By comparing the separation results of the two algorithms, it can be found that the SEPNBD method can achieve the extraction of source signals more accurately than the LBD algorithm.

Nonlinear compensation is the core of the proposed method. To show the superiority of the proposed method in the nonlinear compensation stage, it is compared with the sparsity-based blind compensation method in [18]. The fmincon function in the MATLAB software is used to implement the method. The running time of the method is 4.0342 s, which is the average value of 20 runs. Compared with 0.0279 s of the proposed method, it shows that the proposed method has far superior efficiency.

Nonlinear mixed signals generated by the four nonlinear distortion functions in equation (41) are compensated with the proposed method and the method in [18] respectively, and the noise of different signal-to-noise ratios (SNRs) is applied to compare the compensation performance for different nonlinear distortion functions and the anti-noise performance of different methods. The average SDR of 20 runs is used to evaluate the performance. At each running, the phases of the source signals and the coefficients of the hybrid filter $\boldsymbol{H}$ are regenerated randomly. The results are shown in figure 9. The horizontal axis represents the SNR of the applied noise, and the vertical axis represents the SDR of the compensated signal. Figures 9(a)–(d) correspond to the compensation results of the mixed signals generated by $f_1(u)$, $f_2(u)$, $f_3(u)$, $f_4(u)$ in equation (41), respectively.

As can be seen from figure 9, the compensation results of the proposed method have a higher SDR index. The $L1$-norm based objective function has a better performance than the $L0$-norm based objective function. In addition, the smoothed $L0$-norm introduces the parameter σ, and improper parameter selection also affects the results. By comparing different values of σ, it is found that the results are better when σ is near 0.1. Therefore, the results in figure 9 are all the results under $\sigma = 0.1$. However, the optimal value of σ is different for different signals, so the problem of value σ is also a shortcoming of the method in [18]. These results illustrate that the proposed method has excellent compensation performance.

Through the above comparison, the proposed method is superior in terms of the performance of nonlinear

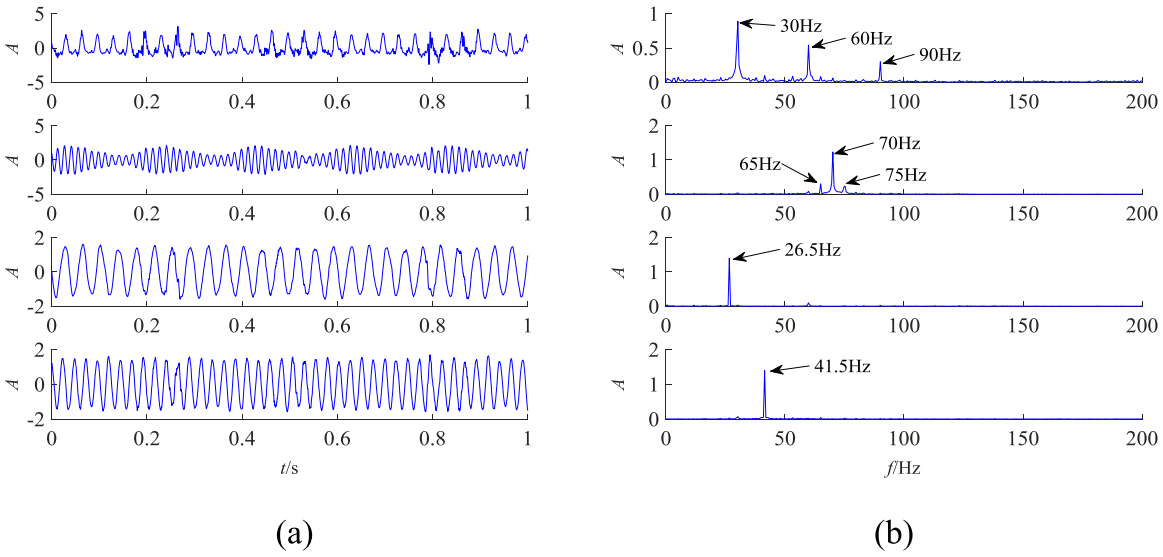

Figure 16. Waveform and spectrums of the separated signals by SEPNBD. (a) Waveforms, (b) Fourier spectrums.

Table 4. Comparison of SCCs of separated signals by different methods.

	SCCs of separated signals				
Methods	$y_1(t)$	$y_2(t)$	$y_3(t)$	$y_4(t)$	Average
Proposed method	0.9540	0.9896	0.9937	0.9919	0.9823
LBD algorithm in [23]	0.6937	0.8982	0.9614	0.9229	0.8691

compensation, the running time of nonlinear compensation and the separation performance.

4. Experimental verification

This paper further tests the effectiveness and superiority of the method by the excitation experiment of the aluminum honeycomb panel cabin structure that simulates the satellite structure.

4.1. Experimental setup

The micro-vibration of the observation camera is an important factor affecting the accuracy of observation satellites. Although the magnitude of satellite micro-vibration is small, its impact is very significant, such as reducing the resolution of earth observation and reducing the pointing precision of space telescopes. The effective identification of the main vibration sources of the satellite has important guiding significance for the vibration reduction measures. As a complex mechanical system, satellite vibration signals are convolutive mixtures of source signals. In addition, when the ground station receives signals from the on-orbit satellite, signals will have serious nonlinear distortion because of the nonlinear characteristic of the satellite channel itself [29]. Therefore, the received satellite micro-vibration signals are post-nonlinear convolutive mixtures.

Referring to the satellite's cabin structure and the characteristics of the main vibration sources, an experimental system of aluminum honeycomb panel cabin structure with four vibration sources is built. The photographs of the experiment system are displayed in figure 10. The scaled model of the satellite cabin structure is designed and manufactured by using the same aluminum honeycomb sandwich panel material and the connection way as the actual satellite according to the actual satellite size. The whole cabin structure model is divided into two cabins by the middle layer of the aluminum honeycomb panel, and the top is a camera simulator. The cabin structure is supported by four air springs to simulate a floating environment and eliminate the influence of ground vibration, as shown in figure 10(a). The vibration sources consist of two vibration exciters and two vibration motors. The output signals of the exciters are controlled by a Tektronix AFG3022C signal generator and the power amplifiers, and the motors are controlled by speed controllers. Vibration signals are measured by PCB356B18 accelerometers installed on the structure surface and recorded by an HBM GEN2i data acquisition system. Figure 10(b) shows the locations of the accelerometers. The experimental control system is shown in figure 10(c).

4.2. Experimental verification of the proposed method

Using the signal collected by the accelerometer when each vibration source operates independently as the source signal, the four source signals of the experiment can be obtained as shown in figure 11, where the first two signals are from exciters and the second two from motors. The sampling frequency is 5000 Hz and the sampling length is 2 s. In order to intuitively show the characteristics of the signals, the waveforms only show the parts of 0–1 s, and the spectrums only show the parts

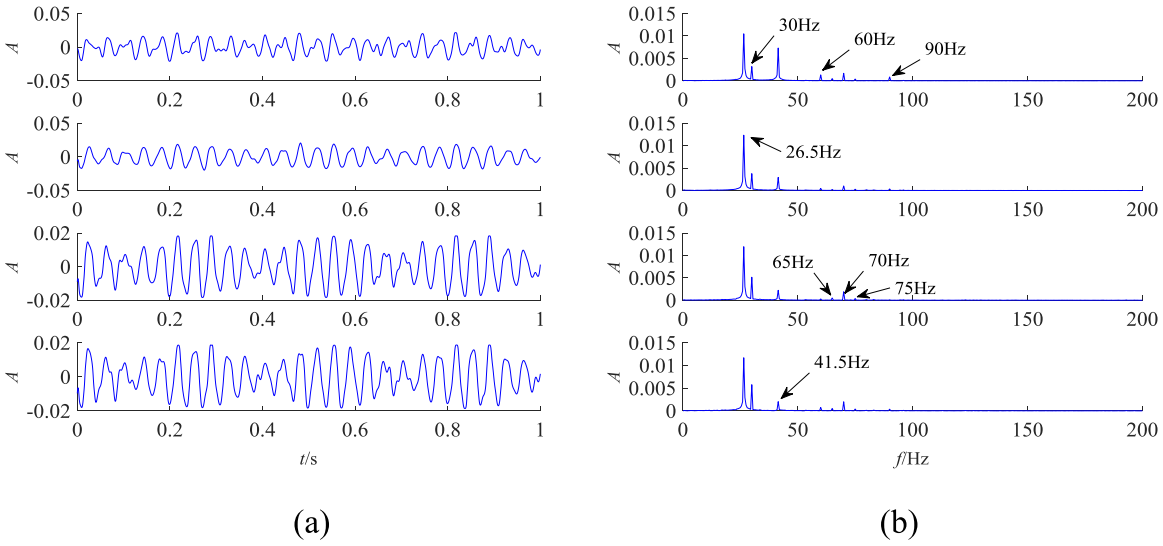

Figure 17. Waveform and spectrums of the compensated signals by the method in [18]. (a) Waveforms, (b) Fourier spectrums.

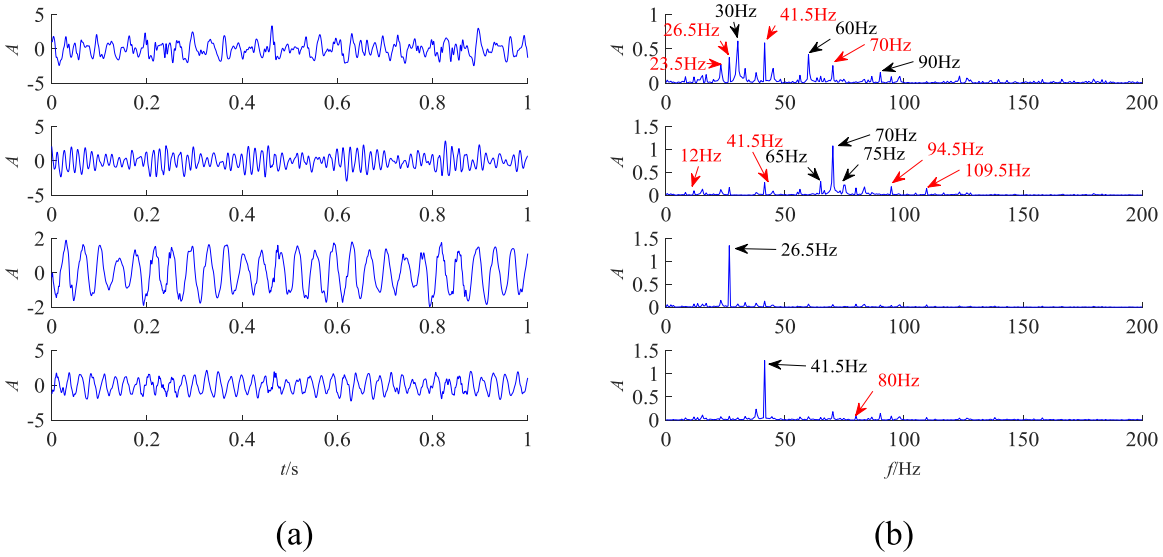

Figure 18. Waveform and spectrums of the separated signals by LBD. (a) Waveforms, (b) Fourier spectrums.

of 0–200 Hz. Mixed signals $\boldsymbol{u}$ collected when four vibration sources operate simultaneously are shown in figure 12. As can be seen, the frequency components of the mixed signals come from each source signal.

The widely used Saleh model [30] is adopted to simulate the amplitude nonlinearity caused by satellite channels. The amplitude model is expressed as follows:

$$f(u) = \alpha u / \left(1 + \beta u^2\right) \tag{44}$$

where α and β are the model parameters, whose values are shown in table 2. The three groups of parameters are given through various experimental data [30].

These three groups of parameters are taken as the parameters of the nonlinear distortion functions of the first three mixed signals respectively, while the third group of parameters is still selected for the fourth mixed signal. Then the curves of the nonlinear distortion functions are shown in figure 13.

Nonlinear distortions are applied to the collected mixed observed signals to simulate the nonlinear distortions of satellite signal reception. The final mixed signals are shown in figure 14. As can be seen from figure 14, besides the frequency components of the source signals, there are many derivative frequency components caused by nonlinear distortion, such as 12 Hz, 23.5 Hz, 94.5 Hz and so on.

The proposed method is used to process the mixed signals. The algorithm parameters are set as follows: the odd polynomial order $p = 4$; smoothing parameter $\delta = 10^{-6}$; iterative step size $\alpha = 0.3$; the threshold value for convergence of nonlinear compensation is 10^{-8}; separation filter length $D = 30$; the maximum number of iterations is 2000; the threshold value for convergence of LBD is 10^{-6}. The waveforms and spectrums of the compensated signals $\boldsymbol{z}$ are shown in figure 15. Comparing figure 14 and 15, it is obvious that the derivative frequency components in figure 14 have been mostly eliminated. The SDRs of the four compensated signals and the running time of nonlinear compensation are listed in table 3. The waveforms and spectrums of the separated signals by SEPNBD are shown in figure 16. By comparing figure 11

and 16, it can be found that the separated signals obtained by the SEPNBD method are consistent with the source signals. The SCCs between the separated signals and the corresponding source signals are listed in table 4. It can be seen that the SEPNBD method successfully achieves the separation of vibration source signals.

4.3. Comparison with other methods

For comparison, the method in [18] is also used to carry out the nonlinear compensation. The compensated signals are shown in figure 17. The derivative frequency components in figure 14 have also been mostly eliminated. The method also achieves satisfactory results. Actually, this method is also an effective algorithm in this application. Table 3 shows the SDRs of compensated signals by different methods. As revealed in table 3, all SDRs of compensated signals obtained by the proposed method are larger. The average SDRs of the proposed method and the method in [18] are 33.12 dB and 28.96 dB respectively. Compared with the two methods, the average SDR improvement of the proposed method is 4.16 dB. Moreover, the running time of the proposed method is 0.1760 s, which is much less than 70.97 s of the method in [18]. The comparisons above indicate that the proposed method is superior to the method in [18] in terms of both the performance and efficiency in the nonlinear compensation stage.

For comparison, the LBD algorithm is used to process the mixed signals in figure 14 directly. The parameters are set as follows: separation filter length $D = 30$; the maximum number of iterations is 2000; the threshold value for convergence is 10^{-6}. The separated signals by the LBD algorithm are obtained as shown in figure 18. As can be seen in figure 18, there are some cross-frequencies such as 26.5 Hz, 41.5 Hz, 70 Hz and some derivative frequencies such as 12 Hz, 23.5 Hz, 94.5 Hz in the Fourier spectrums. The results show that each separated signal of the LBD algorithm still contains components from other sources, and there is much noise of derived frequencies, so the separation of source signals has not been achieved successfully. Table 4 shows the SCCs between the separated signals and the corresponding source signals by different methods. As revealed in table 4, all SCCs obtained by the proposed method are larger. The average SCCs of the proposed method and the LBD algorithm are 0.9823 and 0.8691 respectively. Compared with the two methods, the average SCC improvement of the proposed method is 0.1132, indicating that the proposed method is superior to the LBD algorithm.

The experimental results show that the proposed SEPNBD method can effectively extract the vibration source signals from the post-nonlinear convolutive mixed signals, indicating that the proposed method has the potential to be applied to the identification of satellite micro-vibration sources. Through the comparisons, the superiority of the proposed method in the performance of nonlinear compensation, the efficiency of nonlinear compensation and the separation performance is further verified.

5. Conclusions

In this paper, we propose a new method for post-nonlinear blind deconvolution. The proposed SEPNBD method divides the nonlinear blind deconvolution into two independent steps, i.e. the nonlinear compensation and the linear blind deconvolution. The sparsity enhancement objective function based on $L1$-norm is introduced to the nonlinear compensation stage, which is more robust than the $L0$-norm based objective function and enhances the performance of nonlinear compensation. The fast optimization based on the gradient descent method is presented, which significantly improves the efficiency of the nonlinear compensation stage. The linear blind deconvolution stage is compatible with the well-established blind deconvolution algorithms, making the SEPNBD method have strong adaptability and high accuracy.

To validate the effectiveness and the superiority of the proposed method, some simulation studies and experimental studies on an aluminum honeycomb panel cabin structure are provided. The simulation results show that the proposed SEPNBD method can successfully achieve the separation of vibration source signals from the post-nonlinear convolutive mixtures. Through comparisons with other methods, the proposed method is superior in terms of the performance of nonlinear compensation, the running time of nonlinear compensation and the separation performance. The experimental results further verified the effectiveness. Compared with the nonlinear compensation method in [18], the average SDR of the compensated signals is increased by 4.16 dB. The running time of the proposed method in nonlinear compensation is only 0.1760 s, which remarkably improves the running efficiency. Compared with the LBD algorithm in [23], the average SCC improvement of the proposed method is 0.1132. These results further illustrate the superiority of the proposed method. Therefore, the proposed SEPNBD method is an effective and promising tool in extracting the vibration source signals from the post-nonlinear convolutive mixed signals.

Acknowledgment

This work was supported by the National Natural Science Foundation of China (Grant No: 51775410); and the Science Challenge Project (Grant No: TZ2018007).

ORCID iDs

Zhousuo Zhang https://orcid.org/0000-0003-1299-8974

References

[1] Qin Y, Xing J and Mao Y 2016 Weak transient fault feature extraction based on an optimized Morlet wavelet and kurtosis *Meas. Sci. Technol.* **27** 085003

[2] Li C and Zhan L 2015 A hybrid filtering method based on a novel empirical mode decomposition for friction signals *Meas. Sci. Technol.* **26** 125003
[3] Guo Y *et al* 2018 An optimized variational mode decomposition for extracting weak feature of viscoelastic sandwich cylindrical structures *Meas. Sci. Technol.* **29** 035006
[4] Guo Y *et al* 2018 Generalized variational mode decomposition for interlayer slipping detection of viscoelastic sandwich cylindrical structures *Meas. Sci. Technol.* **29** 095001
[5] Bouguerriou N *et al* 2005 Novel cyclostationarity-based blind source separation algorithm using second order statistical properties: theory and application to the bearing defect diagnosis *Mech. Syst. Signal Process.* **19** 1260–81
[6] Zhang J *et al* 2014 Kurtosis-based constrained independent component analysis and its application on source contribution quantitative estimation *IEEE Trans. Instrum. Meas.* **63** 1842–54
[7] Deville Y and Duarte L T 2015 An overview of blind source separation methods for linear-quadratic and post-nonlinear mixtures *Latent Variable Analysis and Signal Separation* (Cham: Springer) pp 155–67
[8] Taleb A and Jutten C 1999 Source separation in post-nonlinear mixtures *IEEE Trans. Signal Process.* **47** 2807–20
[9] Lu J *et al* 2019 Post-nonlinear blind source separation with kurtosis constraints using augmented Lagrangian particle swarm optimization and its application to mechanical systems *J. Vib. Control.* **25**
[10] Bermejo S 2015 A post-non-linear source separation algorithm for bounded magnitude sources and its application to ISFETs *Neurocomputing* **148** 477–86
[11] Soetraprawata D 2013 Feature extraction of EEG-P300 signals using nonlinear independent component analysis *Int. J. Mech. Mechatronics Eng.* **13** 38–45
[12] Almeida L B 2005 Separating a real-life nonlinear image mixture *J. Mach. Learn. Res.* **6** 1199–229
[13] Corazza G E *et al* 2007 *Digital Satellite Communications* (Boston: Springer) (https://doi.org/10.1007/978-0-387-34649-6)
[14] Duarte L T, Jutten C and Moussaoui S 2010 A Bayesian nonlinear source separation method for smart ion-selective electrode arrays *IEEE Sens. J.* **9** 1763–71
[15] Tsimbinos J and Lever K V 2001 Nonlinear system compensation based on orthogonal polynomial inverses *IEEE Trans. Circuits Syst.* I **48** 406–17
[16] Zhang K and Chan L W 2005 Extended gaussianization method for blind separation of post-nonlinear mixtures *Neural Comput.* **17** 425–52
[17] Dogancay K 2005 Blind compensation of nonlinear distortion for bandlimited signals *IEEE Trans. Circuits Syst.* I **52** 1872–82
[18] Duarte L T *et al* 2015 A sparsity-based method for blind compensation of a memoryless nonlinear distortion: application to ion-selective electrodes *IEEE Sens. J.* **15** 2054–61
[19] Duarte L T *et al* 2012 Blind compensation of nonlinear distortions via sparsity recovery *Proc. 20th Eur. Signal Process. Conf. (EUSIPCO).* pp 2362–66
[20] Donoho D L and Elad M 2003 Optimally sparse representation in general (nonorthogonal) dictionaries via L1 minimization *Proc. Natl Acad. Sci.* **100** 2197–202
[21] Thomas J, Deville Y and Hosseini S 2006 Time-domain fast fixed-point algorithms for convolutive ICA *IEEE Signal Process. Lett.* **13** 228–31
[22] Belaid S *et al* 2016 A new multi-scale framework for convolutive blind source separation *Signal Image Video Process.* **10** 1203–10
[23] Castella M and Moreau E 2012 New kurtosis optimization schemes for MISO equalization *IEEE Trans. Signal Process.* **60** 1319–30
[24] Loubaton P and Regalia P A 1993 Blind deconvolution of multivariate signals: a deflation approach *1993 IEEE Int. Conf. on Communications* pp 1160–64
[25] Bishop C M 2006 *Pattern Recognition and Machine Learning* (New York: Springer) (https://doi.org/10.1117/1.2819119)
[26] Hyvärinen A and Oja E 2000 Independent component analysis: algorithms and applications *Neural Netw.* **13** 411–30
[27] Dubroca R *et al* 2010 A general algebraic algorithm for blind extraction of one source in a MIMO convolutive mixture *IEEE Trans. Signal Process.* **58** 2484–93
[28] Newland D E 1993 Harmonic wavelet analysis *Proc. R. Soc.* A **443** 203–25
[29] Colavolpe G, Modenini A and Rusek F 2012 Channel shortening for nonlinear satellite channels *IEEE Commun. Lett.* **16** 1929–32
[30] Saleh A A M 1981 Frequency-independent and frequency-dependent nonlinear models of TWT amplifiers *IEEE Trans. Commun.* **29** 1715–20